Journal of Advanced Ceramics
2020, **9**(6): 683–692
https://doi.org/10.1007/s40145-020-0404-7

ISSN 2226-4108
CN 10-1154/TQ

Research Article

Fabrication and electrical characteristics of flash-sintered SiO_2-doped $ZnO–Bi_2O_3–MnO_2$ varistors

Pai PENG[a,b], Yujun DENG[a,b], Jingpeng NIU[a,b], Liyi SHI[c], Yunzhu MEI[a,b], Sanming DU[d], Juan LIU[a,b,*], Dong XU[a,b,*]

[a]*Key Laboratory of Green Fabrication and Surface Technology of Advanced Metal Materials (Anhui University of Technology), Ministry of Education, Ma'anshan 243002, China*
[b]*Key Laboratory of Etallurgical Emission Reduction & Resources Recycling (Anhui University of Technology), Ministry of Education, Ma'anshan 243002, China*
[c]*Research Center of Nano Science and Technology, Shanghai University, Shanghai 200444, China*
[d]*National United Engineering Laboratory for Advanced Bearing Tribology, Henan University of Science and Technology, Luoyang 471023, China*

Received: April 22, 2020; Revised: July 2, 2020; Accepted: July 4, 2020

Abstract: The dense $ZnO–Bi_2O_3–MnO_2–xSiO_2$ (ZBMS) varistors for x = 0, 1, 2, 3 wt% were fabricated by flash sintering method under the low temperature of 850 ℃ within 2 min. The sample temperature was estimated by a black body radiation model in the flash sintering process. The crystalline phase assemblage, density, microstructure, and electrical characteristics of the flash-sintered ZBMS varistors with different SiO_2-doped content were investigated. According to the XRD analysis, many secondary phases were detected due to the SiO_2 doping. Meanwhile, the average grain size decrease with increasing SiO_2-doped content. The improved nonlinear characteristics were obtained in SiO_2-doped samples, which can be attributed to the ion migration and oxygen absorption induced by the doped SiO_2. The flash-sintered ZBMS varistor ceramics for x = 2 wt% exhibited excellent comprehensive electrical properties, with the nonlinear coefficient of 24.5, the threshold voltage and leakage current of 385 V·mm^{-1} and 11.8 μA, respectively.

Keywords: flash sintering; SiO_2 additive; ZBMS varistors; electrical properties

1 Introduction

ZnO varistors have been successfully applied to the surge protector in electrical transmission and transient overvoltage or circuits to prevent lightning strikes due to their excellent nonlinearly electrical characteristics which originate from the grain boundaries [1]. It is generally believed that ZnO varistors are made by mixing zinc oxide powders with various oxide additives, such as Bi_2O_3 [2,3], Sb_2O_3 [4,5], Co_2O_3 [6,7], Sc_2O_3 [8], MnO_2 [9], Cr_2O_3 [10,11], and TiO_2 [12]. At present, most ZnO-based varistors are prepared by a conventional sintering method. However, it needs high sintering temperature (about 1200 ℃) and long holding time (> 2 h), leading to high energy consumption [13,14]. Besides, the high sintering temperature may lead to the

* Corresponding authors.
E-mail: J. Liu, jliu0922@ahut.edu.cn;
D. Xu, frank@shu.edu.cn

volatilization of some elements (like Bi), which in turn affects the varistor properties. Thus, it is necessary to find a new sintering method with low sintering temperature and short sintering time.

Recently, a new sintering method, flash sintering (FS), has been reported, which can reduce the furnace temperature required for sintering 3 mol% yttria-stabilized zirconia (3YSZ) from 1450 to 850 ℃, and greatly shorten the time to around 5 s [15]. The combination of furnace temperature and electric field promotes the FS for the preparation of ceramics. Compared with other sintering methods, the FS time is extremely short (about seconds), which is nearly negligible in contrast to the number of hours required by the conventional sintering (CS). Therefore, the flash technique has attracted significant scientific and technical attention. Since its first discovery, the FS method has been widely applied to the preparation for a variety of ceramics, including ionic conductors (YSZ) [16–18] and CeO_2 [19,20], electronic conductors (TiO_2) [21,22], ferroelectrics ($BaTiO_3$) [23,24], semiconductors and varistors (ZnO) [25,26], perovskites ($SrTiO_3$) [27,28], insulators (Al_2O_3 and Y_2O_3) [29,30]. The mechanisms of the flash sintering have been proposed by many researchers. It is generally believed that the Joule heating is caused by flowing current during the FS process [31], contributing to the reduction of sintering temperature. Besides, because it is difficult to measure the sample temperature in the flash sintering process, the sample temperature (T, in K) can be estimated by the Black Body Radiation (BBR) model [32], and the sample temperature can be calculated by Eq. (1):

$$T = \left(T_0^4 + \frac{W}{A\varepsilon\sigma} \right)^{1/4} \quad (1)$$

where T_0 is the onset flash furnace temperature (K), W is the power dissipation in the unit of $W \cdot m^{-3}$, A is the surface area of the sample (1.429×10^{-4} m^2), ε is the emissivity, and $\sigma = 5.67 \times 10^{-8}$ $W \cdot m^{-2} \cdot K^{-4}$ is the Stefan–Boltzmann constant.

Based on the above discussion, ZnO varistors can be prepared by the flash sintering method. For example, Zhang and Luo [26] prepared ZnO specimen by flash sintering method at low furnace temperature (< 120 ℃). In fact, a lot of reports have been investigated on the flash sintering for the preparation of ZnO ceramics [33,34]. However, the research mainly focuses on the flash sintering of pure zinc oxide, and there are few investigations on the ZnO-based varistor. Recently, the ZnO–Bi_2O_3–MnO_2 varistors have been fabricated by the flash sintering at a very low sintering temperature of 768–702 ℃ under an electric field of 200–400 $V \cdot cm^{-1}$, which showed an excellent nonlinear property [35]. The dense ZnO–Bi_2O_3–M (M = Cr_2O_3, MnO_2, or Co_2O_3) ceramics were obtained by flash sintering at a low temperature (< 750 ℃) with the highest nonlinear coefficient of 39.5 [36]. In ZnO–Bi_2O_3–MnO_2 varistors, Bi_2O_3 acts as Double Schottky Barrier (DSB) to form at the grain boundary layers, which provides the medium for the liquid phase to wet the grain boundary regions [37]. Meanwhile, the doping of transition metal oxide (MnO_2) increases the grain boundary barrier and affects the migration of carriers. The potential barrier is not only related to the ion migration, but also to the oxygen adsorption. It is demonstrated that oxygen can be generated by a chemical defect reaction of silica and zinc oxide [38]. In addition, the Zn ions in the ZnO crystal are replaced by Si ions, forming two positively charged centers Si_{Zn}^{2+} and improving the ability to bind electrons. The ionic radius of Si is 0.26 Å. Si^{4+} enters into the continuous path more easily than other transition metal ions. Besides, the density of traps can be significantly enhanced by SiO_2, which may promote the varistor characteristics and flash sintering process.

According to the above discussions, it is very meaningful to explore the effect of different SiO_2 content on the structure and electrical properties of ZnO–Bi_2O_3–MnO_2-based varistor prepared by flash sintering. In present work, the dense ZnO–Bi_2O_3–MnO_2–$xSiO_2$ varistors were fabricated by the flash sintering method at a temperature of 850 ℃ within 2 min. The flash parameters on sintering were investigated, including current, voltage, power density, and conductivity. The specimen temperature was estimated by the black body radiation model during the flash event.

2 Experimental details

2. 1 Preparation of green specimens

ZnO, Bi_2O_3, MnO_2, and SiO_2 analytical-grade chemicals were purchased from Sinopharm (Beijing, China) and the materials were used as received. The chemical formula was 98 mol% ZnO + 1.0 mol% Bi_2O_3 + 1.0 mol% MnO_2 + $xSiO_2$ (x = 0–3 wt%). Firstly, the starting materials were mixed with the right amount of ethanol in a zirconia ball mill. The oxide mixture was subsequently milled for 5 h and then dried at 70 ℃ for

24 h. Secondly, all powders were mixed with 5 wt% polyvinyl alcohol (PVA) as a binder and after uniaxially pressed in a pellet at about 310 MPa for 3 min. Thereafter, the powders shaped green samples with a dimension of about 7 mm diameter and about 3 mm thickness. Finally, the green sample was calcined at 500 ℃ for 2 h to remove the binder. The densities of the green samples were in a range of 55%–57%.

2. 2 Flash process

The specimen was placed in a retrofitted tube furnace (OTF-1200X-S, KJ Group, China) with two platinum wires, which were also connected to the electrodes sandwiched between the two sections of the specimen. Subsequently, the specimen was added electric field by a direct-current (DC) (Sorenson DLM-300, Sorensen, CA) and the furnace heating rate at 10 ℃·min^{-1} heated to 850 ℃. Specifically, due to local sintering in the flash process, a gradient increased current was used in the experiment. Firstly, the applied electrical field (E) was 300 V·cm^{-1}, and the initial limit current (I_0) was set to be 1.0 A. Thereafter, when the limit current was reached, the current was maintained for 10 s and then increased to 1.5 A. Similarly until the maximum current (I_{max}) was reached to 3.0 A, the flash sintering process continued for 10 s. Finally, the power supply system and the tube furnace were turned off, and then the specimen was cooled within the furnace to room temperature. The experimental parameters during the flash sintering process were shown in Table 1.

2. 3 Characterization

The structure of the flash-sintered specimens was studied by X-ray diffraction (XRD, D8 Advance, Germany). The electron probe microanalyzer (SEM, NANO SEM430, USA) was used to observe the sample microstructure. The density of flash-sintered samples was measured and calculated by the Archimedes method. The silver paste was applied as an electrode to the sample surface. The I–V characteristics of the flash-sintered sample were measured by a digital electrometer (CJ 1001, China) with a DC source. The varistor voltage (U_{1mA}) and the leakage current (I_L) at 75% U_{1mA} of ZBMS varistors were measured at room temperature. More generally, the nonlinear coefficient (α) can be calculated according to the following Eq. (2):

$$\alpha = \frac{\log(I_{1mA} / I_{0.1mA})}{\log(U_{1mA} / U_{0.1mA})} = \frac{1}{\log(U_{1mA} / U_{0.1mA})} \quad (2)$$

where U_{1mA} and $U_{0.1mA}$ are the varistor voltage at 1 and 0.1 mA, respectively. The frequency-dependent dielectric properties were characterized via a capacitance meter (Agilent 4294A, USA) in the frequency range of 10^3–10^6 Hz at room temperature.

Table 1 Experimental parameters of flash sintering

x (wt%)	E (V·cm^{-1})	I_0 (A)	I_{max} (A)	FS condition
0–3	300	1.0	3.0	0.5 A/10 s

3 Results and discussion

3. 1 Variation of flash parameters on sintering

The curves of (a) current, (b) voltage, (c) power density, and (d) conductivity versus time during the flash sintering process were shown in Fig. 1. Zero-point was the time when the current reached a preset value. The current increased from 1.0 to 3.0 A with a gradient way (Fig. 1(a)). As shown in Fig. 1(b), the voltage dropped sharply from 90 V to about 20 V when the current surged to 1.0 A. Thereafter, the voltage tended to be a stable state gradually and then increased with the increasing current. When the current reached to the maximum value, the voltage was kept at about 63 V. Figure 1(c) highlights the power density as functions of time during the FS process. The power density was calculated according to $P = IU/V$, where U is the voltage, I is the current, and V is the sample's volume. Subsequently, the power density curve had the same trend as the variations of current and voltage because the power density is the combination of the voltage and current. As shown in Fig. 1(d), the specimen conductivity increased sharply when the flash was triggered. Here, the conductivity can be calculated by the equation $\sigma = IH/US$, where I is the current, H is the height of the sample, U is the voltage, and S is the sample's cross-sectional area. When the current was small (1.0–2.0 A), the conductivity increased with the increase of current. On the other hand, the conductivity decreased again because the rate of voltage increase was greater than that of the current when the current was large (2.0–3.0 A). Besides, the reduction of conductivity may be attributed to the high resistance formed by the grain boundary barrier during the FS process.

3. 2 Measurements and estimates of the specimen temperature

Figure 2(a) reveals the estimated temperature of x =

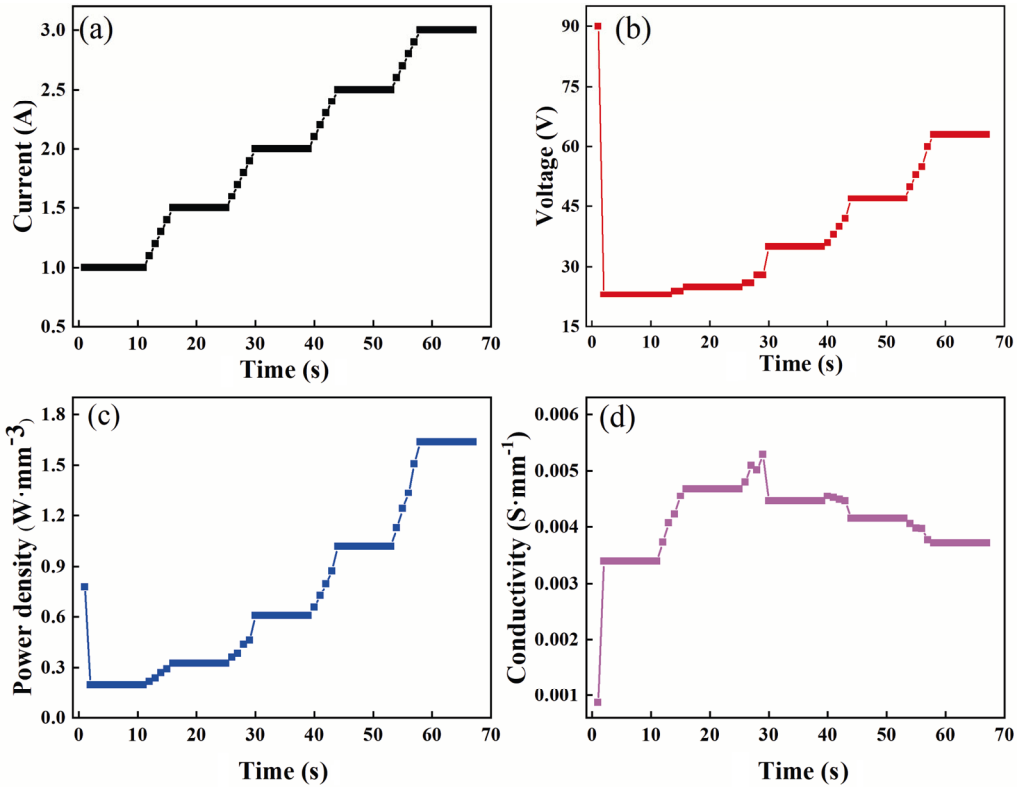

Fig. 1 (a) Current, (b) voltage, (c) power density, and (d) conductivity versus time during flash sintering.

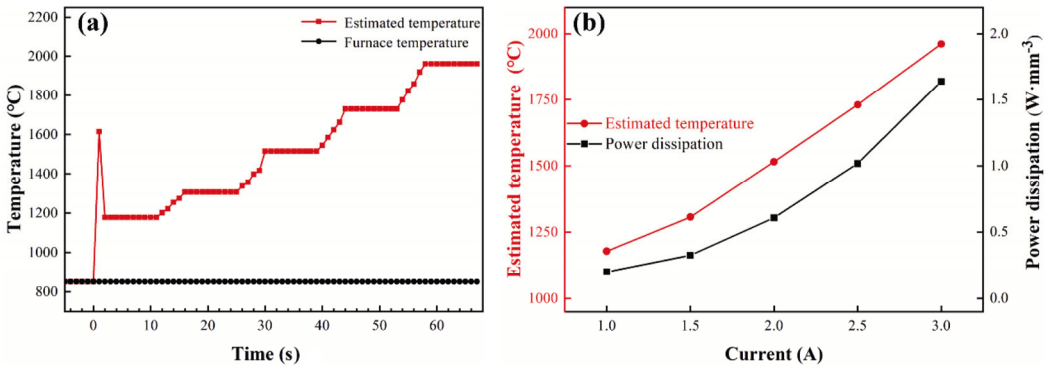

Fig. 2 (a) Estimated sample temperature versus time during flash sintering at x = 1 wt%. (b) Estimating sample temperature and power dissipation as a function of current with a preset maximum current of 3.0 A.

1 wt% sample versus time during the flash sintering process, and the estimated sample temperature can be calculated by the black body radiation (BBR) model (Eq. (1)). The specimen temperature was the same as the furnace temperature before the electric field was applied. When the flash was triggered, the peak temperature can reach around 1600 ℃. When the voltage control was converted to the current control model, the specimen temperature dropped to about 1200 ℃ [32,39]. The result shows that the heating rate of temperature was about 10^4 ℃·min^{-1}, and the sample temperature was extremely higher than the furnace temperature. Furthermore, the temperature increased with the increasing current. After the current reached the pre-set value, the current increased in a gradient way. In particular, when the current reached the maximum value, the estimated specimen temperature reached to higher than 1950 ℃. At this stage, the average heating rate was about 2×10^3 ℃·min^{-1}. The specimen temperature heating rate greatly decreased after the flash, which made the temperature of the specimen more uniform during the FS process and solved the problem of local sintering. Figure 2(b) depicts the estimated sample temperature and power dissipation as a function of current at x = 1 wt%. Apparently, the estimated

specimen temperature and the power dissipation increased linearly with the increasing current, and a positive correlation between the estimated specimen temperature and the power dissipation was observed, which indicated that the sintering was strongly dependent on the Joule heating generated during the flash process. Besides, the estimated temperature was much higher than the required furnace temperature for conventional sintering, which indicated that high temperature was also an important factor for the rapid densification of ceramics.

3. 3 Phase structure, density, and microstructure

The crystal structures of flash-sintered ZBM–$x$$SiO_2$ ceramics were characterized via XRD, and the results were shown in Fig. 3. Obviously, the main phase of all flash-sintered samples was the ZnO phase (PDF No. 36.1451). Except for ZnO phase, many extra diffraction peaks were detected which can be identified as Bi_2O_3 phase (PDF No. 41.1449), $Bi_{12}SiO_{20}$ glass phase (PDF No. 37.0485), and Zn_2SiO_4 phase (PDF No. 37.1485) (Fig. 3). Owing to that the radius of Bi ions (r = 1.03 Å) was larger than that of Zn ions (r = 0.74 Å), more Bi_2O_3 existed in the grain boundary layer. In addition, because MnO_2 and ZnO may form a solid solution, no diffraction peaks about Mn ions were found. It is worth noting that the type of secondary phase was related to the doping content of SiO_2. When the doping content was 1 wt%, the secondary phase was mainly $Bi_{12}SiO_{20}$ and Bi_2O_3. When the doping content increased to 2 wt%, Bi_2O_3, Zn_2SiO_4, and $Bi_{12}SiO_{20}$ phases can be identified in these compositions. Since the radius of Si ions (r = 0.26 Å) was smaller than that of Zn ions (r = 0.74 Å),

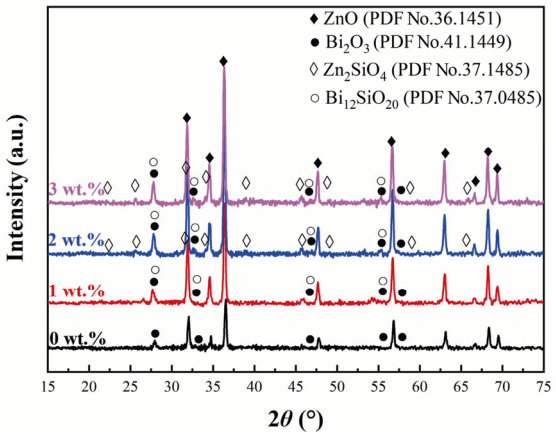

Fig. 3 XRD patterns of flash-sintered samples with different SiO_2-doped content under the electrical field of 300 V·cm^{-1}.

Si ions entered into the lattice of ZnO grains when x was lower than 1 wt%. In the case of $x \geqslant 2$ wt%, Si ions may segregate at the grain boundary and lead to the formation of Zn_2SiO_4 phase.

The relative density of all flash-sintered ZBM–$x$$SiO_2$ varistors was measured and listed in Table 2, and the values of the relative density for x = 0, 1, 2, and 3 wt% samples were 97.8%, 98.4%, 97.1%, and 94.3%, respectively. Clearly, the relative density increased first and then decreased with the increase SiO_2 in doping content. It indicated that the proper addition of SiO_2 can form glass phase at the grain boundary, thereby improving the wet ability of the grain boundary, enhancing the surface tension of the Bi-rich liquid phase, accelerating the particle flow rate in the sample, promoting the rearrangement process, and increasing the accumulation density and densification degree of particles in the sample. However, owing to that the density of SiO_2 (2.63 g·cm^{-3}) is much lower than that of ZnO (5.67 g·cm^{-3}), excessive SiO_2 will lead to the decreasing of the density [40]. On the other hand, the Zn_2SiO_4 phase may reduce the growth speed of ZnO grains and eventually decrease the density. More details were found in the following discussion.

The microscopic morphologies of the flash-sintered ZBM–$x$$SiO_2$ ceramics were shown in Fig. 4. Clearly, the grain size decreased with increasing SiO_2 doping content. The decrease in grain size led to an increase in the grain boundary, which eventually increased the threshold voltage. This is consistent with the results in Table 2. The decreased grain size can be attributed to the doping with SiO_2, which promoted the formation of the glass phase with other additives at high temperatures. Then, the Zn_2SiO_4 spinel phase was condensed in the cooling process, and mainly distributed at the grain boundary. Similar to the mechanism of the $Zn_7Sb_2O_{12}$ phase, the Zn_2SiO_4 phase acted as a nail at the grain boundary, thus hindering grain movement and inhibiting grain growth [40]. In addition, taking the 3 wt% sample as an example, the effect of the electrode on the

Table 2 Electrical properties and relative density of flash-sintered samples with different SiO_2-doped content under the electrical field of 300 V·cm^{-1}

x (wt%)	Relative density	I_L (μA)	V_T (V·mm^{-1})	α	φ_B (eV)
0	97.8%	8.48	234	20.1	0.76
1	98.4%	8.43	375	22.2	0.89
2	97.1%	11.8	385	24.5	0.80
3	94.3%	58.7	498	12.2	0.78

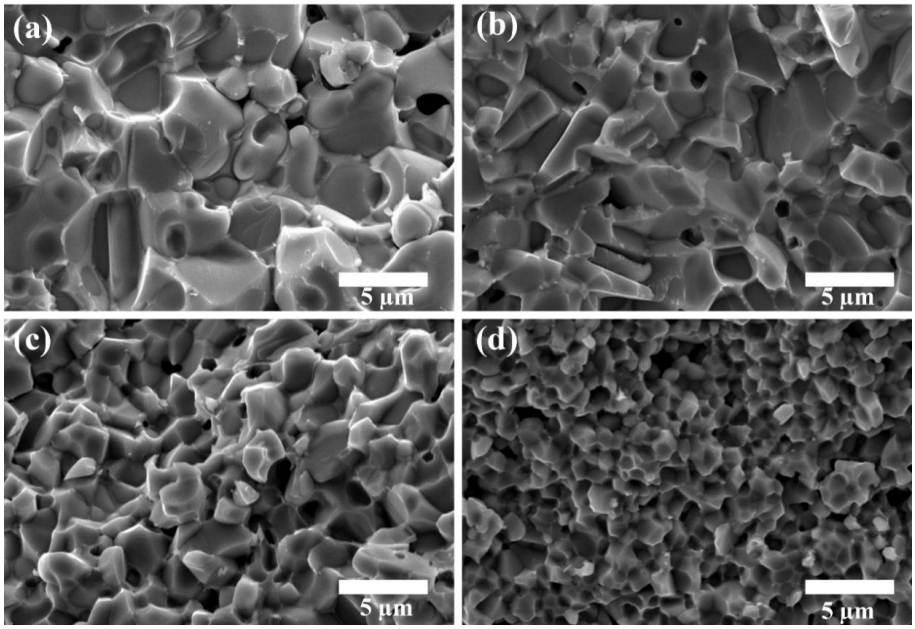

Fig. 4 SEM patterns of flash-sintered samples with different SiO_2-doped content: (a) 0 wt%, (b) 1 wt%, (c) 2 wt%, (d) 3 wt%.

microstructure was investigated. The microstructures on both sides of the flash-sintered sample electrode were shown in Fig. 5. Apparently, the grain size on both sides of the electrode did not change obviously, which is consistent with the previous reports [35].

3. 4 Electrical properties

Figure 6(a) shows the *E*–*J* curves of flash-sintered samples doped with different SiO_2 contents. Obviously, all samples exhibited nonlinear properties. The variation of nonlinear coefficient (α) and a threshold voltage (V_T) of the ZBM–$x$$SiO_2$ varistors were shown in Fig. 6(b). Meanwhile, the electrical properties of flash-sintered samples were evaluated and listed in Table 2. As shown in Fig. 6(b), the nonlinear coefficient and a threshold voltage of ZBMS varistors were enhanced by doping with SiO_2. The optimal nonlinear characteristics were obtained in 2 wt% sample with a value of 24.5. The threshold voltage increased significantly with increasing SiO_2 content, and the largest threshold voltage was obtained at x = 3 wt% sample with a value of 498 $V{\cdot}mm^{-1}$. Moreover, the varistor voltage depended on grain size according to Eq. (3) [41]:

$$U_{1mA} = N_{gb}V_{gb} \tag{3}$$

where N_{gb} is the number of grain boundaries and V_{gb} is the average voltage per grain boundary. When the content of SiO_2 increased from 1 to 3 wt%, the grain size gradually decreased, that is, the number of grain boundaries per unit thickness increased, and the threshold voltage gradually increased. However, the nonlinear coefficient decreased to 12.2, and the leakage current increased significantly to 58.7 μA at x = 3 wt%. The deteriorated nonlinear properties at this sample were ascribed to the excessive SiO_2, which is because the excessive SiO_2 may form a large number of secondary phases. The increased leakage current was attributed to

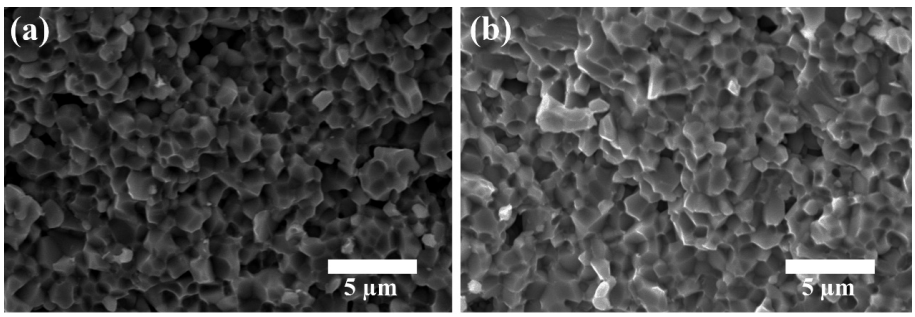

Fig. 5 SEM images of the flash-sintered sample on both sides of the electrode: (a) anode (+), (b) cathode (–) at x = 3 wt%.

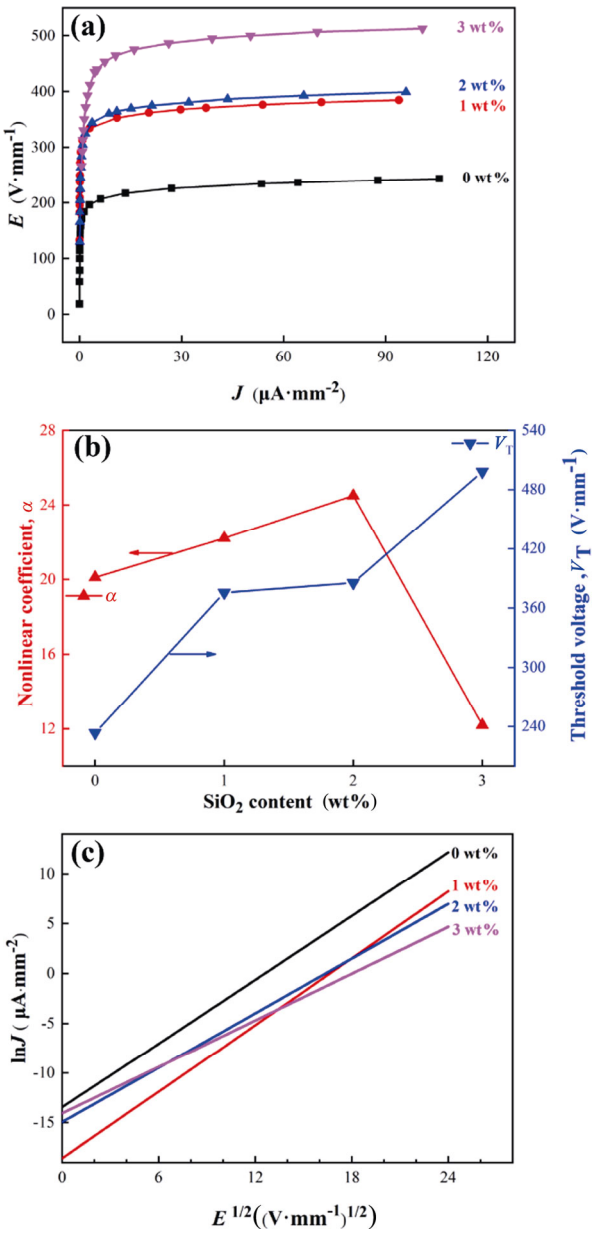

Fig. 6 (a) *E*–*J* curve of flash-sintered samples with different SiO_2-doped content. (b) Variation of nonlinear coefficient and threshold voltage of the flash-sintered ZBM–*x*SiO_2 varistors (*x* = 0–3 wt%). (c) ln*J*–$E^{1/2}$ curves of flash-sintered ZBM–*x*SiO_2 (*x* = 0–3 wt%) varistors.

the increased conductivity of the grain boundary layer, while the increased conductivity was attributed to the intergranular phase (Bi_2O_3, Zn_2SiO_4, and $Bi_{12}SiO_{20}$) formed by a large amount of SiO_2 [42–44]. In addition, the leakage current of the samples may have a certain relationship with the relative density, where the larger the density, the smaller the leakage current. When the specimen was under a low electric field, electrons cross the Schottky Barrier to generate a thermal excitation current, which is related to the electric field as Eq. (4) [45]:

$$J_s = A^* \cdot T^2 \cdot \exp[(\beta E^{1/2} - \varphi_B)/kT] \quad (4)$$

where A^* is the Richardson's constant, k is the Boltzmann constant, E is the electric field, φ_B is the barrier voltage, and β satisfies Eq. (5) [45]:

$$\beta \propto 1/(r * \omega) \quad (5)$$

where r is the number of grains per unit length, ω is the barrier width. Based on the natural logarithm of Eq. (5), the ln*J*–$E^{1/2}$ curves of flash-sintered ZBM–*x*SiO_2 ceramics were calculated and displayed in Fig. 6(c). It was found that ln*J* changes linearly with the increase of $E^{1/2}$, then a linear fit was performed, and the fitted line extended to $E = 0$. As shown in Fig. 6(c), the slope of the $\ln J \propto E^{1/2}$ curves was β/kT, and the intercept was the difference between a constant and the barrier heights.

The values of barrier voltage which were fitted by Eq. (5) were listed in Table 2. When the content of SiO_2 increased from 0 to 3 wt%, the barrier voltage was 0.76, 0.89, 0.80, and 0.78 eV, respectively. The enhanced barrier voltage can be attributed to the doping with SiO_2, which can form the glass phase with Bi_2O_3 at the grain boundary in the flash sintering process. The wetting effect of the liquid phase can be improved at the grain boundary. Moreover, it also affected the segregation concentration of the extrinsic surface impurities on the grain surface, which increased the grain boundary barrier. The defect reactions of SiO_2 and ZnO can be represented by Kroger–Vink symbols:

$$SiO_2 \xrightarrow{ZnO} Si_{Zn}^{\times} + V_{Zn}^{\times} + O_2$$

$$SiO_2 \xrightarrow{Bi_2O_3} Si^{4-} + 4e^- + O_2$$

$$O_2 \rightarrow 2O_{ad}$$

$$O_{ad} + e^- \rightarrow O_{ad}^-$$

$$O_{ad} + 2e^- \rightarrow O_{ad}^{2-}$$

$$Zn_i^{\cdot} + O_{ad}^- \rightarrow ZnO$$

$$Zn_i^{\cdot\cdot} + O_{ad}^{2-} \rightarrow ZnO$$

When ZnO was undoped with SiO_2, the defect structure was mainly composed of MnO_2 related solution diffusion reaction. When the ZnO varistors were doped with SiO_2, oxygen was generated due to the chemical defect reaction between SiO_2, ZnO, and Bi_2O_3, resulting in an increase in the adsorbed oxygen content. After that, a large

number of free electrons migrated toward the grain boundary, resulting in a significant increase in the width of the depletion layer and a decrease of intrinsic donor defects $Zn_i^{\cdot}$ and $Zn_i^{\cdot\cdot}$. Furthermore, due to that the Si^{4+} ion radius (0.26 Å) is smaller than those of Zn^{2+} (0.74 Å) and Mn^{4+} (0.53 Å), it will preferentially diffuse in the ZnO lattice, and may reduce the diffusion rate of Mn^{4+}. As a result, the solid solution reaction on the grain surface was enhanced, the formation of grain boundary was promoted, the grain boundary barrier was increased, and the nonlinear characteristics were improved [38].

Figure 7 features the frequency-dependent dielectric characteristics of the flash-sintered ZBM–$x$$SiO_2$ varistors (x = 0–3 wt%) at room temperature. As shown in Fig. 7, the doped SiO_2 led to a decrease in dielectric constant (ε') and an increase in dielectric loss (tanδ) at low frequency. With the increase of SiO_2 doping content, the grain size decreased and the depletion layer width increased, resulting in a decrease in dielectric constant. Meanwhile, the dielectric constant showed a certain frequency dependence, which decreased with the increasing frequency. Especially for x = 0 wt%, the dielectric constant decreased rapidly at above 10^5 Hz (Fig. 7(a)). Interestingly, the frequency stability enhanced with increasing of SiO_2-doped content. Moreover, the dielectric loss was mainly caused by Joule heating which generated from leakage current and eddy current heat which originated from electric dipole moment rotation [46]. The dielectric loss was high at x = 3 wt%, which may be attributed to the large leakage current (Fig. 7(b)).

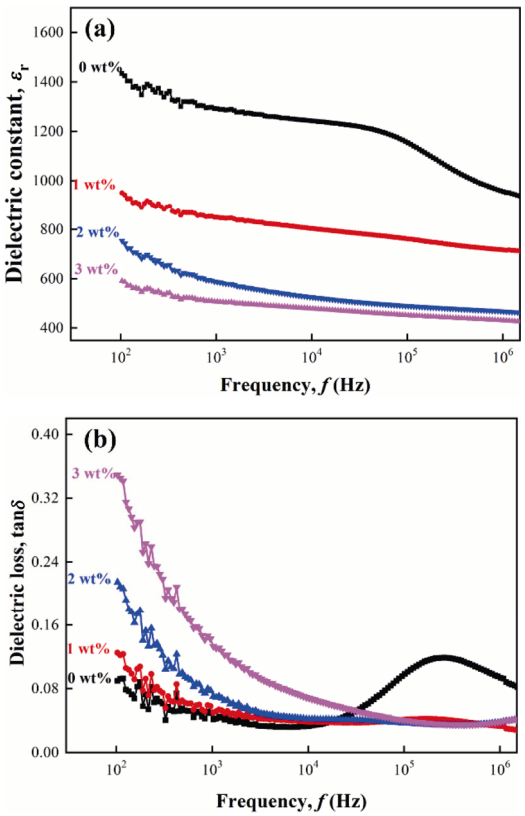

Fig. 7 Dielectric properties of the flash-sintered ZBM–$x$$SiO_2$ varistors (x = 0–3 wt%) as a function of frequency with a preset maximum current of 3.0 A: (a) dielectric constant (ε'), (b) dielectric loss (tanδ).

4 Conclusions

The dense ZBM–$x$$SiO_2$ varistors for x = 0, 1, 2, 3 wt% were prepared by flash sintering method under a low temperature of 850 ℃ within 2 min. The temperature of the samples was estimated by the black body radiation model during the FS process. The effects of SiO_2 contents on the structure and properties of ZnO-based varistors were investigated. Except for ZnO main phase, some secondary phases induced by doping with SiO_2 were detected. Meanwhile, the grain size decreased, which can be attributed to the inhibition of grain growth by the secondary phase. The electrical performance analysis of the flash-sintered specimens showed that the electrical properties were improved by doping with SiO_2. The improved nonlinear electrical properties can be ascribed to the ion migration and oxygen absorption. The flash-sintered ZBMS varistor exhibited excellent comprehensive electrical properties at x = 2 wt%, with a nonlinear coefficient of 24.5, a threshold voltage of 385 V·mm^{-1}, and a leakage current of 11.8 μA. Therefore, the flash sintering method is a promising method for preparing ceramics, and there are still many works to be investigated in the future.

Acknowledgements

This work was financially supported by National Natural Science Foundation of China (Grant Nos. 51802003 and 51572113), State Key Laboratory of New Ceramic and Fine Processing Tsinghua University (No. KF201808), and the Project National United Engineering Laboratory for Advanced Bearing Tribology (No. 201912).

References

[1] Wong J. Sintering and varistor characteristics of ZnO–Bi_2O_3 ceramics. *J Appl Phys* 1980, **51**: 4453–4459.

[2] Szwagierczak D, Kulawik J, Skwarek A. Influence of processing on microstructure and electrical characteristics of multilayer varistors. *J Adv Ceram* 2019, **8**: 408–417.
[3] Xu D, Shi LY, Wu ZH, *et al*. Microstructure and electrical properties of ZnO–Bi_2O_3-based varistor ceramics by different sintering processes. *J Eur Ceram Soc* 2009, **29**: 1789–1794.
[4] Liu FH, Xu GJ, Duan L, *et al*. Influence of B_2O_3 additives on microstructure and electrical properties of ZnO–Bi_2O_3–Sb_2O_3-based varistors. *J Alloys Compd* 2011, **509**: L56–L58.
[5] Ott J, Lorenz A, Harrer M, *et al*. The influence of Bi_2O_3 and Sb_2O_3 on the electrical properties of ZnO-based varistors. *J Electroceramics* 2001, **6**: 135–146.
[6] Kim ED, Kim CH, Oh MH. Role and effect of Co_2O_3 additive on the upturn characteristics of ZnO varistors. *J Appl Phys* 1985, **58**: 3231–3235.
[7] Ezhilvalavan S, Kutty TRN. Dependence of non-linearity coefficients on transition metal oxide concentration in simplified compositions of ZnO+Bi_2O_3+MO varistor ceramics (M = Co or Mn). *J Mater Sci: Mater Electron* 1996, **7**: 137–148.
[8] Xu D, Cheng XN, Zhao GP, *et al*. Microstructure and electrical properties of Sc_2O_3-doped ZnO–Bi_2O_3-based varistor ceramics. *Ceram Int* 2011, **37**: 701–706.
[9] Jiang F, Peng ZJ, Zang YX, *et al*. Progress on rare-earth doped ZnO-based varistor materials. *J Adv Ceram* 2013, **2**: 201–212.
[10] Kanai H, Imai M. Effects of SiO_2 and Cr_2O_3 on the formation process of ZnO varistors. *J Mater Sci* 1988, **23**: 4379–4382.
[11] Kim YH, Kawamura H, Nawata M. The effect of Cr_2O_3 additive on the electrical properties of ZnO varistor. *J Mater Sci* 1997, **32**: 1665–1670.
[12] Bernik S, Daneu N, Rečnik A. Inversion boundary induced grain growth in TiO_2 or Sb_2O_3 doped ZnO-based varistor ceramics. *J Eur Ceram Soc* 2004, **24**: 3703–3708.
[13] Khafagy AMH, El-Rabaie SM, Dawoud MT, *et al*. Microhardness, microstructure and electrical properties of ZVM ceramics. *J Adv Ceram* 2014, **3**: 287–296.
[14] Szwagierczak D, Kulawik J, Skwarek A. Influence of processing on microstructure and electrical characteristics of multilayer varistors. *J Adv Ceram* 2019, **8**: 408–417.
[15] Cologna M, Rashkova B, Raj R. Flash sintering of nanograin zirconia in <5 s at 850 ℃. *J Am Ceram Soc* 2010, **93**: 3556–3559.
[16] Jha SK, Terauds K, Lebrun JM, *et al*. Beyond flash sintering in 3 mol% yttria stabilized zirconia. *J Ceram Soc Jpn* 2016, **124**: 283–288.
[17] Qin W, Yun J, Thron AM, *et al*. Temperature gradient and microstructure evolution in AC flash sintering of 3 mol% yttria-stabilized zirconia. *Mater Manuf Process* 2017, **32**: 549–556.
[18] Zhang J, Wang ZH, Jiang TZ, *et al*. Densification of 8 mol% yttria-stabilized zirconia at low temperature by flash sintering technique for solid oxide fuel cells. *Ceram Int* 2017, **43**: 14037–14043.
[19] Guan LL, Li J, Song XW, *et al*. Graphite assisted flash sintering of Sm_2O_3 doped CeO_2 ceramics at the onset temperature of 25 ℃. *Scripta Mater* 2019, **159**: 72–75.
[20] Jha SK, Charalambous H, Wang H, *et al*. *In-situ* observation of oxygen mobility and abnormal lattice expansion in ceria during flash sintering. *Ceram Int* 2018, **44**: 15362–15369.
[21] Charalambous H, Jha SK, Wang H, *et al*. Inhomogeneous reduction and its relation to grain growth of titania during flash sintering. *Scripta Mater* 2018, **155**: 37–40.
[22] Charalambous H, Jha SK, Wang H, *et al*. Inhomogeneous reduction and its relation to grain growth of titania during flash sintering. *Scripta Mater* 2018, **155**: 37–40.
[23] Shi RK, Pu YP, Wang W, *et al*. Flash sintering of Barium titanate. *Ceram Int* 2019, **45**: 7085–7089.
[24] Ma BS, Zhu Y, Wang KW, *et al*. Microstructure and dielectric property of flash sintered SiO_2-coated $BaTiO_3$ ceramics. *Scripta Mater* 2019, **170**: 1–5.
[25] Charalambous H, Jha SK, Lay RT, *et al*. Investigation of temperature approximation methods during flash sintering of ZnO. *Ceram Int* 2018, **44**: 6162–6169.
[26] Zhang YY, Luo J. Promoting the flash sintering of ZnO in reduced atmospheres to achieve nearly full densities at furnace temperatures of <120 ℃. *Scripta Mater* 2015, **106**: 26–29.
[27] Lemke F, Rheinheimer W, Hoffmann MJ. A comparison of power controlled flash sintering and conventional sintering of strontium titanate. *Scripta Mater* 2017, **130**: 187–190.
[28] Karakuscu A, Cologna M, Yarotski D, *et al*. Defect structure of flash-sintered strontium titanate. *J Am Ceram Soc* 2012, **95**: 2531–2536.
[29] Liu DG, Gao Y, Liu JL, *et al*. Preparation of Al_2O_3–$Y_3Al_5O_{12}$–ZrO_2 eutectic ceramic by flash sintering. *Scripta Mater* 2016, **114**: 108–111.
[30] Zhang H, Wang YG, Liu JL, *et al*. Reaction assisted flash sintering of Al_2O_3–YAG ceramic composites with eutectic composition. *Ceram Int* 2019, **45**: 13551–13555.
[31] Dong YH, Chen IW. Thermal runaway in mold-assisted flash sintering. *J Am Ceram Soc* 2016, **99**: 2889–2894.
[32] Raj R. Joule heating during flash-sintering. *J Eur Ceram Soc* 2012, **32**: 2293–2301.
[33] Zhang YY, Luo J. Promoting the flash sintering of ZnO in reduced atmospheres to achieve nearly full densities at furnace temperatures of <120 ℃. *Scripta Mater* 2015, **106**: 26–29.
[34] Nie JY, Zhang YY, Chan JM, *et al*. Water-assisted flash sintering: Flashing ZnO at room temperature to achieve ~98% density in seconds. *Scripta Mater* 2018, **142**: 79–82.
[35] Mei YZ, Pandey S, Long WM, *et al*. Processing and characterizations of flash sintered ZnO–Bi_2O_3–MnO_2 varistor ceramics under different electric fields. *J Eur Ceram Soc* 2020, **40**: 1330–1337.
[36] Cui B, Niu JP, Peng P, *et al*. Flash sintering preparation and electrical properties of ZnO–Bi_2O_3–M (M = Cr_2O_3, MnO_2 or Co_2O_3) varistor ceramics. *Ceram Int* 2020, **46**: 14913–

14918.

[37] Xu D, Cheng XN, Yan XH, *et al*. Sintering process as relevant parameter for Bi_2O_3 vaporization from ZnO–Bi_2O_3-based varistor ceramics. *Trans Nonferrous Met Soc China* 2009, **19**: 1526–1532.

[38] Bai HR, Li MM, Xu ZJ, *et al*. Influence of SiO_2 on electrical properties of the highly nonlinear ZnO–Bi_2O_3–MnO_2 varistors. *J Eur Ceram Soc* 2017, **37**: 3965–3971.

[39] Schmerbauch C, Gonzalez-Julian J, Röder R, *et al*. Flash sintering of nanocrystalline zinc oxide and its influence on microstructure and defect formation. *J Am Ceram Soc* 2014, **97**: 1728–1735.

[40] Canikoğlu N, Toplan N, Yıldız K, *et al*. Densification and grain growth of SiO_2-doped ZnO. *Ceram Int* 2006, **32**: 127–132.

[41] Levinson LM, Philipp HR. Zinc oxide varistors—a review. *Am Ceram Soc Bull* 1986, **65**: 639–646..

[42] Xu D, Yue XN, Zhang YD, *et al*. Enhanced dielectric properties and electrical responses of cobalt-doped $CaCu_3Ti_4O_{12}$ thin films. *J Alloys Compd* 2019, **773**: 853–859.

[43] Xu D, Yue XN, Song J, *et al*. Improved dielectric and non-ohmic properties of (Zn + Zr) codoped $CaCu_3Ti_4O_{12}$ thin films. *Ceram Int* 2019, **45**: 11421–11427.

[44] Yue XN, Long WM, Liu J, *et al*. Enhancement of dielectric and non-ohmic properties of graded Co doped $CaCu_3Ti_4O_{12}$ thin films. *J Alloys Compd* 2020, **816**: 152582.

[45] Dhage SR, Ravi V, Yang OB. Low voltage varistor ceramics based on SnO_2. *Bull Mater Sci* 2007, **30**: 583–586.

[46] Nahm CW, Shin BC, Min BH. Microstructure and electrical properties of Y_2O_3-doped ZnO–Pr_6O_{11}-based varistor ceramics. *Mater Chem Phys* 2003, **82**: 157–164.